PREECLAMPSIA

Protein misfolding, congophilia, oligomerization, and defective amyloid processing in preeclampsia

Irina A. Buhimschi,[1,2]* Unzila A. Nayeri,[2] Guomao Zhao,[1] Lydia L. Shook,[2] Anna Pensalfini,[3] Edmund F. Funai,[4] Ira M. Bernstein,[5] Charles G. Glabe,[6,7] Catalin S. Buhimschi[2,4]

Preeclampsia is a pregnancy-specific disorder of unknown etiology and a leading contributor to maternal and perinatal morbidity and mortality worldwide. Because there is no cure other than delivery, preeclampsia is the leading cause of iatrogenic preterm birth. We show that preeclampsia shares pathophysiologic features with recognized protein misfolding disorders. These features include urine congophilia (affinity for the amyloidophilic dye Congo red), affinity for conformational state–dependent antibodies, and dysregulation of prototype proteolytic enzymes involved in amyloid precursor protein (APP) processing. Assessment of global protein misfolding load in pregnancy based on urine congophilia (Congo red dot test) carries diagnostic and prognostic potential for preeclampsia. We used conformational state–dependent antibodies to demonstrate the presence of generic supramolecular assemblies (prefibrillar oligomers and annular protofibrils), which vary in quantitative and qualitative representation with preeclampsia severity. In the first attempt to characterize the preeclampsia misfoldome, we report that the urine congophilic material includes proteoforms of ceruloplasmin, immunoglobulin free light chains, SERPINA1, albumin, interferon-inducible protein 6-16, and Alzheimer's β-amyloid. The human placenta abundantly expresses APP along with prototype APP-processing enzymes, of which the α-secretase ADAM10, the β-secretases BACE1 and BACE2, and the γ-secretase presenilin-1 were all up-regulated in preeclampsia. The presence of β-amyloid aggregates in placentas of women with preeclampsia and fetal growth restriction further supports the notion that this condition should join the growing list of protein conformational disorders. If these aggregates play a pathophysiologic role, our findings may lead to treatment for preeclampsia.

INTRODUCTION

Preeclampsia (PE) is a human-specific pregnancy disorder of unknown etiology. If left untreated, patients may have a progressive clinical deterioration resulting in seizures (eclampsia), stroke, hemorrhage, kidney damage, liver failure, and death. The World Health Organization (WHO) estimates that worldwide ~63,000 women die annually because of PE (*1*). Most of these deaths occur in low- and mid-income countries and are often caused by a delay or lack of diagnosis.

The clinical syndrome of PE is defined as new-onset hypertension and proteinuria after 20 weeks of gestation (*2*). This rule applies to most, but not all, cases (*3*). One major issue is the unpredictability of PE in its clinical presentation and speed of progression. Early clinical signs of PE are frequently inconspicuous, and the effectiveness of hypertension and proteinuria as diagnostic "gold standard" is compromised when PE is superimposed on other predisposing conditions, such as chronic hypertension (crHTN) or nephropathy.

The central role played by the placenta in the pathophysiology of PE has emerged from the observation that the only definitive treatment for this condition is early delivery of the fetus and the placenta (*4*). Oxidative stress, vascular endothelial dysfunction, systemic inflammation, altered levels of nitric oxide (NO), and aberrant angiogenesis are some of the pathologic processes known to be involved (*5*). Much research has focused on the exploration of a panel of coagulation, inflammatory, and angiogenic protein mediators for diagnosing PE (*6*–*9*). However, most studies using a "candidate marker" approach have had the disadvantage of restricting the search to known proteins that can be either up- or down-regulated (*6*). By using an unbiased mass spectrometry proteomic profiling approach, we discovered that urine of women with severe PE (sPE) requiring medically indicated delivery (MIDPE) displayed a characteristic set of proteomic biomarkers consisting of nonrandom proteoforms of SERPINA1 and albumin (*10*). This feature had diagnostic and prognostic potential, because it preceded the onset of clinical manifestations and correlated with disease severity (*10*). Consistent with the existent evidence that some SERPINA1 fragments have the propensity to misfold and aggregate into supramolecular structures (*11*), we formulated the hypothesis that PE shares pathophysiologic characteristics with known protein conformational disorders. Herein, we demonstrated that urine of PE women exhibits congophilia, a characteristic of protein misfolding (*12*). We used conformational state antibodies that recognize mutually exclusive generic epitopes associated with prefibrillar oligomers (PFOs), annular protofibrils (APFs; structurally and functionally distinct oligomers in ring-shaped, pore-like conformation), or fibrils and fibrillar oligomers (*13*–*15*) to confirm the presence of nonrandom protein aggregation in the urine of women with PE. Reasoning that excess fragments of SERPINA1 and albumin may result from a proteolytic-antiproteolytic imbalance (*16*) analogous to that generating Alzheimer's β-amyloid (Aβ) from the ubiquitously expressed amyloid precursor protein (APP) (*17*), we searched for dysregulation in the expression of prototype α-, β-, and γ-secretases in the placenta of PE women. Last, we demonstrated the presence of APP-derived amyloid-like proteins in the urine and placenta of women with PE.

[1]Center for Perinatal Research, The Research Institute at Nationwide Children's Hospital and Department of Pediatrics, The Ohio State University College of Medicine, Columbus, OH 43215, USA. [2]Department of Obstetrics, Gynecology and Reproductive Sciences, Yale University School of Medicine, New Haven, CT 06520, USA. [3]Center for Dementia Research, Nathan Kline Institute for Psychiatric Research and Department of Psychiatry, New York University School of Medicine, New York, NY 10016, USA. [4]Department of Obstetrics and Gynecology, The Ohio State University College of Medicine, Columbus, OH 43210, USA. [5]Department of Obstetrics, Gynecology and Reproductive Sciences, University of Vermont College of Medicine, Burlington, VT 05405, USA. [6]Department of Molecular Biology and Biochemistry, University of California, Irvine, Irvine, CA 92617, USA. [7]Department of Biochemistry and Experimental Biochemistry Unit, King Abdulaziz University, Jeddah 22254, Saudi Arabia.
*Corresponding author. E-mail: irina.buhimschi@nationwidechildrens.org

RESULTS

Women with sPE exhibit urine congophilia with spectral features of amyloid-like aggregates

We tested our hypothesis by using a study design with feasibility and validation phases (Fig. 1). As initial proof of principle (feasibility), we tested urine samples from pregnant women (n = 80) with precise clinical classifications and known outcomes: 40 sPE women requiring MIDPE and 40 healthy pregnant controls (P-CRL) who had an uncomplicated gestation and delivered at term. Their clinical characteristics are included in table S1. We designed a simple method whereby urine that had been mixed with Congo red (CR) was spotted on an unsupported nitrocellulose membrane, which was then washed with increasing concentrations of methanol (Fig. 2A). The rationale of this experiment was based on the self-assembling property of CR and its ability to initiate formation of large insoluble oligomers after binding to amyloid proteins that have an extensive β sheet structure (*18*). As shown, spots of urine from sPE, but not P-CRL, women remained red after the methanol wash, indicating that women with PE display urinary congophilia. A standardized protocol was designed to allow an objective quantification of each urine sample's propensity to retain CR and minimize variations because of differences in proteinuria and hydration status (the CRD test). Two indices were obtained through image analysis: CRI (the reference measure of the initial redness of the spot) and CRR (measure of congophilia as the redness of spot after removing unbound CR). No differences in CRI were noted between the two groups (Fig. 2B). However, compared to P-CRL, CRR was significantly increased in sPE urine (P < 0.001, Fig. 2C). In receiver operating curve characteristic (ROC) analysis of our feasibility cohort, a CRR cutoff value of 15% had 100% [95% confidence interval (CI), 92 to 100] sensitivity and 100% [95% CI, 92 to 100] specificity to discriminate sPE cases from P-CRLs. On the basis of this result, we considered CRR ≥15% as "nonreassuring" (NR-CRR).

CR-bound amyloids exhibit bright red fluorescence and shift their absorbance from about 490 to 540 nm when illuminated with UV light (*19*). Upon illumination of our nitrocellulose membrane with long- but not short-wavelength UV, we observed the characteristic red fluorescence of amyloid-bound CR (Fig. 2D). Immediately upon addition of CR stock solution, we noted that 30% (12 of 40) of sPE urine samples (but no P-CRLs) changed color from orange-red to magenta (Fig. 2E), consistent with the bathochromic spectral shift described for Aβ oligomerization (aggregation) in vitro (*20*). Spectrophotometric determination

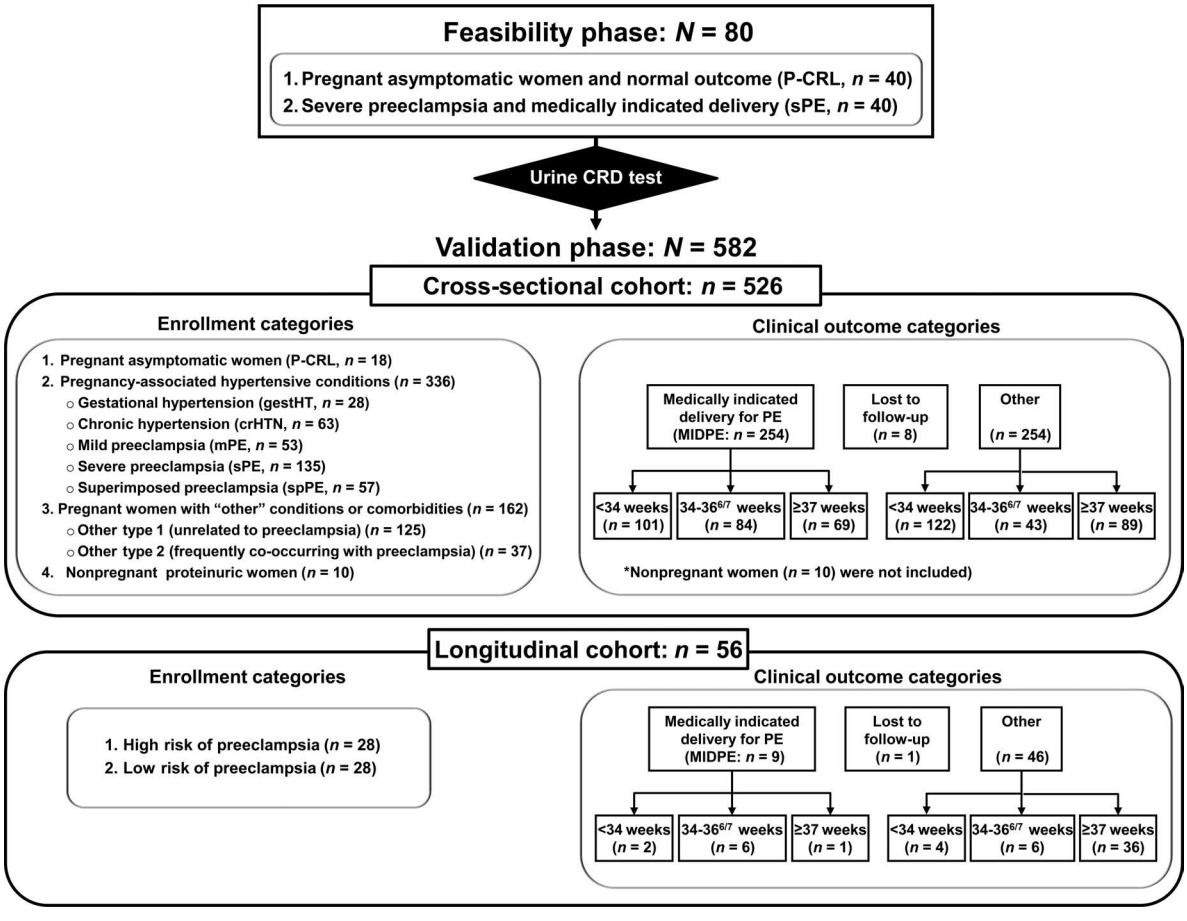

Fig. 1. Flow chart of the study design and women who donated urine samples for the urine Congo red dot (CRD) test. A total of 662 women donated urine samples for the current study. The initial feasibility phase included samples from 80 women that had either a normal pregnancy or clear clinical manifestations of early-onset sPE that required MIDPE. The remaining samples were used for the validation phase and to calculate the diagnostic and prognostic characteristics of our urine CRD test. Cases were analyzed by the outcome relevant to our study (MIDPE) at different gestational age (GA) periods: early preterm (<34 weeks), near term (34 to $36^{6/7}$ weeks), and term (≥37 weeks).

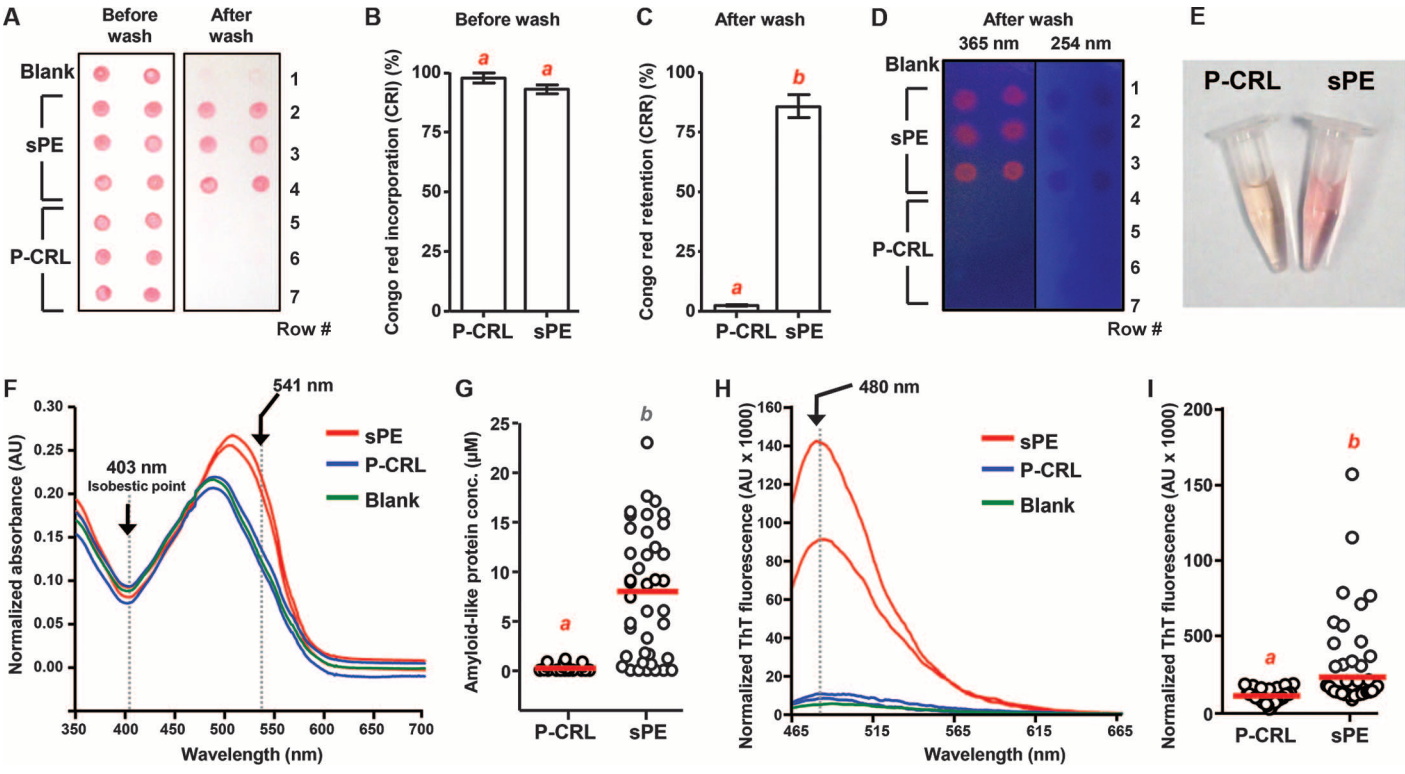

Fig. 2. Spectral characteristics of protein aggregation and congophilia in urine of women with sPE. (**A**) Representative CRD test result of urine from three sPE women (lanes 2 to 4) and three healthy P-CRLs from the feasibility cohort (lanes 5 to 7). Urine was mixed with a solution of CR and spotted in duplicate on a strip of nitrocellulose, which was photographed before and after washing with increasing concentration of methanol. Lane 1 was spotted with a solution of phosphate buffer saline (blank). The spots corresponding to sPE urine retained the red color, whereas P-CRL spots washed away. (**B** and **C**) The two images in (A) were sequentially photographed, and the amount of CR retained after the wash within each spot was calculated as the percent of the amount present before the wash. (B) The amount of CR before the wash was calculated as an internal control index [CR incorporation (CRI)] for the P-CRL (n = 40) and sPE (n = 40) urine samples in the feasibility phase and was not different between the two groups. (C) The test output [CR retention (CRR)], measure of urine congophilia, was markedly elevated in sPE group. (**D**) Photograph of the same nitrocellulose sheet after the wash, illuminated with either long-wavelength (365 nm) or short-wavelength (254 nm) ultraviolet (UV) light. (**E**) Some, but not all, sPE urine samples turned magenta when mixed with CR. This change was visually notable for urine samples with high CRR indices and corresponded to the bathochromic shift described upon binding of CR to β sheet structures. (**F**) The bathochromic shift can be quantified objectively by measuring the absorbance at 541 nm (point of maximal shift) after normalization (subtraction of absorbance in the respective sample without CR). The two red lines are normalized representative spectra from urine of two patients with sPE. The blue lines correspond to spectra from two P-CRL urine samples. AU, arbitrary units. (**G**) Scatter plot of congophilia determined by direct spectrophotometry. (**H**) Thioflavin T (ThT)–induced fluorescence of urine samples analyzed in the feasibility phase. Spectra from two sPE women (red lines) and two P-CRL women (blue lines) are displayed. (**I**) Scatter plot of ThT-induced fluorescence determined by spectrofluorimetry (excitation: 444 nm/emission: 480 nm). Red horizontal bars represent group medians. Red superscripts indicate groups with statistically significant differences at $P < 0.05$ (B and C: Student's t test; G and I: Mann-Whitney test). Exact P values are provided in table S6.

of absorbencies at 403 nm (isobestic point) and 541 nm (point of maximal shift) confirmed the presence of amyloid-like aggregates in sPE urine (Fig. 2F). Although as a group, sPE women had a higher concentration of amyloid-like aggregates, 20% (8 of 40) of sPE urines did not exhibit a detectable (visual and/or spectrophotometric) spectral shift despite NR-CRR in the CRD test (Fig. 2G). A spectrophotometrically detectable shift occurred only for samples with CRR >50%, implying that compared to CRD test (CRR cutoff 15%), direct spectrophotometry has a lower sensitivity [80% (95% CI, 64 to 91)] in identifying PE (P = 0.007, feasibility cohort). In addition, sPE women exhibited increased urine ThT–induced fluorescence (Fig. 2H, $P < 0.001$), another indicator that amyloid-like structures were present in the urine of women with PE. Similar to direct spectrophotometry, only a subgroup of sPE specimens (42%) showed an increase in fluorescence upon ThT binding (Fig. 2I). Compared to the CRD test, urine ThT binding had a lower sensitivity [82% (95% CI, 65 to 92)] in identifying PE ($P < 0.001$, feasibility cohort).

Urine congophilia differs among hypertensive pregnancy disorders and increases with PE severity

To further understand the clinical implication of urine congophilia during pregnancy, we tested urine samples from an additional 582 women, this time unselected with respect to enrollment category (Fig. 1, validation phase). A cross-sectional (n = 526) and a longitudinal (n = 56) cohort were designed. Women in the cross-sectional cohort participated with a single urine sample. The results were grouped and analyzed on the basis of clinical classification at sample collection and pregnancy outcome (MIDPE or other). The clinical characteristics of

the women included in the cross-sectional cohort are presented in table S2. Women in the longitudinal cohort were asymptomatic for PE at study entry and were followed throughout gestation.

When cases enrolled in the cross-sectional cohort were grouped by clinical diagnosis at the time of sample collection, both sPE and superimposed PE (spPE; PE superimposed on preexisting hypertension or proteinuria) women had higher CRR compared to all other groups (Fig. 3A, $P < 0.001$). Next, we analyzed the proportion of women displaying urine NR-CRR values. We found that 75% (40 of 53), 89% (120 of 135), and 91% (52 of 57) of women admitted with a diagnosis of mild PE (mPE), sPE, and spPE, respectively, had NR-CRR values (Fig. 3B). These proportions were significantly higher than in all the other groups ($P < 0.05$). Among crHTN women ruled out for spPE based on clinical and laboratory criteria at the time of enrollment, 35% (22 of 63) displayed NR-CRR. This was significantly higher compared to P-CRLs (6%, 1 of 18, $P = 0.017$) or women with pathologies unrelated to PE (grouped as other type 1 conditions: 13%, 16 of 125, $P < 0.001$). Details on clinical definitions and criteria for patient classification are included in Supplementary Materials and Methods. Consistent with the progressing nature of PE, 27% (17 of 63) of women classified as crHTN at enrollment had their diagnosis revised to spPE and ultimately required MIDPE (Fig. 3C). Of these, 53% (9 of 17) had urine congophilia at the initial evaluation, implying that the CRD test may be useful for rapidly predicting spPE when this condition cannot

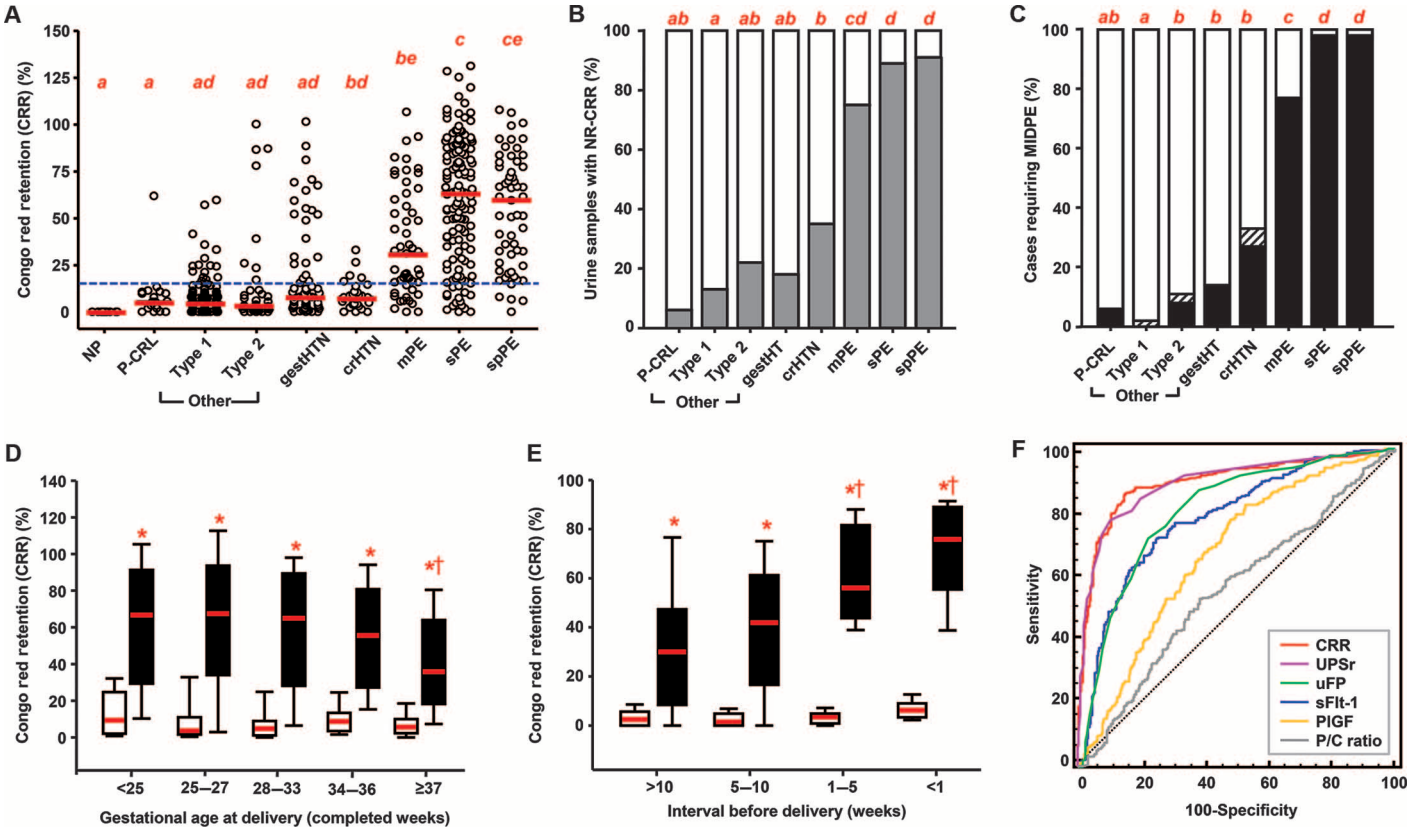

Fig. 3. Diagnostic and prognostic features of urine congophilia. (**A**) Scatter plots of CRR for the cross-sectional validation cohort ($n = 526$) by enrollment diagnoses: nonpregnant (NP, $n = 10$), P-CRL ($n = 18$), other type 1 conditions ($n = 125$), other type 2 conditions ($n = 37$), gestational hypertension (gestHTN, $n = 28$), crHTN ($n = 63$), mPE ($n = 53$), sPE ($n = 135$), and spPE ($n = 57$). Red lines mark groups' medians. The blue dotted line marks the 15% cutoff in CRR. (**B**) Proportion of pregnant subjects in the cross-sectional validation phase cohort ($n = 516$) with NR-CRR values (CRR ≥15%, gray portion of the bars) grouped by enrollment diagnoses. (**C**) Proportion of pregnant women in the same cohort that ultimately required MIDPE (black portion of the bars, $n = 254$). Hashed portions correspond to cases lost to follow-up ($n = 8$). (**D**) Urine CRR values for the cross-sectional validation phase cohort grouped by GA at delivery ($n = 508$ subjects with known outcomes). MIDPE cases (black boxes): 20 to 24 weeks ($n = 15$), 25 to 27 weeks ($n = 22$), 28 to 33 weeks ($n = 64$), 34 to 36 weeks ($n = 84$), and 37 to 41 weeks ($n = 69$). Cases with outcomes deemed clinically unrelated to PE (open boxes): <20 weeks ($n = 19$), 25 to 27 weeks ($n = 28$), 28 to 33 weeks ($n = 75$), 34 to 36 weeks ($n = 43$), and 37 to 41 weeks ($n = 89$). (**E**) CRR values of the longitudinal cohort ($n = 55$ women with known outcomes) grouped by time intervals to delivery. MIDPE cases (black boxes, $n = 9$); women who did not develop PE (open boxes, $n = 46$). (**F**) ROC for prediction of MIDPE among pregnant subjects in the validation cohort with known outcomes ($n = 563$). Each subject participated with a single specimen (earliest available). CRR's performance was compared with that of urine proteomics score (UPSr), soluble fms-like tyrosine kinase-1 (sFlt-1)/placental growth factor (PlGF) ratio (known as uFP), creatinine-normalized sFlt-1, creatinine-normalized PlGF, and protein-to-creatinine ratio (P/C ratio). (A to C) Groups sharing at least one common red letter are not statistically different at $P > 0.05$ [A: Kruskal-Wallis analysis of variance (ANOVA) with Dunn's post hoc tests; B and C: χ^2 tests]. (D and E) Red lines mark groups' median. The limits of the box mark the 25 and 75 centiles. The whiskers extend between 5 and 95 centiles. Asterisks note significant differences ($P < 0.05$) between MIDPE and non-MIDPE groups for each period. Daggers note significant differences from the first period within each group (two-way ANOVA followed by Holm-Sidak tests). Exact P values are provided in table S6.

be diagnosed based on the current clinical criteria alone. The relationship between CRR index and MIDPE in the longitudinal cohort is presented in Fig. 3D, grouped by GA at delivery. Women who required MIDPE had significantly higher CRR at all GA periods (two-way ANOVA: MIDPE, $P < 0.001$; GA, $P = 0.008$; interaction, $P = 0.018$). Among women managed with MIDPE, CRR levels were significantly higher in preterm PE compared to term PE ($P < 0.001$). This may be explained by the higher representation of mPE at term, which is managed by MIDPE without delay, in accordance with the standard of care. Additionally, cases with high CRR (≥60%) were less represented in women with term MIDPE compared to those requiring MIDPE at <34 weeks (29% versus 58%, $P = 0.003$).

In our longitudinal cohort (Fig. 3E), women who developed PE requiring MIDPE ($n = 9$, all from the high-risk enrollment group) had significantly higher CRR before clinical manifestation of the disease ($P < 0.001$ for both MIDPE and interval to delivery). Seven of nine (78%) of these women had NR-CRR values at study entry, more than 10 weeks before clinically overt PE. This suggests that the underlying mechanism of urine congophilia likely occurs early in the asymptomatic phase and worsens progressively. Overall, four high-risk women displayed urine congophilia at <20 weeks GA, and all had MIDPE. All the low-risk women ($n = 28$) had a pregnancy course uncomplicated by PE and term delivery, and all but one remained non-congophilic throughout pregnancy. This one case became congophilic in the third trimester and underwent indicated delivery for gestHTN at term.

Among low- and high-risk women who did not develop PE, there was no statistical difference in CRR at study entry (low risk: 3.2 ± 0.6% versus high risk: 7.0 ± 2.8%, $P = 0.397$).

The CRD test is a simple modality to diagnose sPE and predict MIDPE

ROC analysis of enrollment urine samples ($n = 563$) from the pregnant women included in the validation cohort who had known pregnancy outcomes (cross-sectional cohort subjects not lost to follow-up: $n = 508$ + longitudinal cohort subjects not lost to follow-up: $n = 55$) determined that CRR alone (cutoff of ≥15%) had a sensitivity of 85.9% (95% CI, 81.1 to 89.9), specificity of 85.0% (95% CI, 80.4 to 88.8), positive likelihood ratio (LR) of 5.7 (95% CI, 4.4 to 7.5), and negative LR of 0.17 (95% CI, 0.1 to 0.2) in predicting PE requiring MIDPE (table S3). This was significantly better compared to the currently recognized clinical screening criteria for diagnosis of PE (CRR versus blood pressure: $P < 0.001$; CRR versus protein dipstick: $P < 0.001$). CRR had additive value to both systolic and diastolic blood pressures ($P < 0.001$). CRR alone performed significantly better than the combination of blood pressure and proteinuria based on the recommended cutoffs of both American College of Obstetricians and Gynecologists ($P = 0.004$) (*2*) and WHO ($P < 0.001$) (*21*). The association of CRR with MIDPE remained significant after controlling for GA and maternal demographic characteristics in multiple logistic regression [NR-CRR odds ratio (95% CI), 30.6 (18.9 to 49.6); GA odds ratio, 3.3 (2.0 to 5.4)]. Maternal age, race, and parity were excluded from the model on the basis of $P > 0.1$.

Next, we analyzed the group of women who completed 24-hour urine protein collections (gold standard for proteinuria of PE, $n = 250$). We found a significant correlation between CRR and 24-hour proteinuria ($r = 0.788$, $P < 0.001$). Of the women with 24-hour proteinuria (≥300 mg/24 hours) that required MIDPE, 94% (148 of 158) had CRR ≥15%, and 82% (129 of 158) had CRR ≥30% (fig. S1). We further noted that a number of PE cases deemed "atypical" ($n = 40$) based on the absence of either proteinuria or hypertension displayed urine congophilia. Of the nonproteinuric atypical cases, 58% (23 of 40) were congophilic at the time of first evaluation, suggesting the potential clinical usefulness of the CRD test in such clinical circumstances. All 23 congophilic women with "atypical PE" had a medically indicated delivery. In 21 cases, the delivery indication was sPE with atypical presentation. In the remaining two cases, the indication for delivery was documented as abnormal fetal heart rate tracing.

CRR performed significantly better than urine sFlt-1/PlGF ratio (*22*) (z statistic = 4.5, $P < 0.001$), creatinine-normalized urine sFlt-1 concentration (z statistic = 6.8, $P < 0.001$), creatinine-normalized urine PlGF concentration (z statistic = 9.2, $P < 0.001$), and P/C ratio (z statistic = 13.9, $P < 0.001$) (Fig. 3F). CRR had similar performance in predicting MIDPE with our previously described UPSr (z statistic = 0.4, $P = 0.695$) (*10*). The proteomics score was the strongest predictor of urine congophilia among women who required MIDPE, independent of GA or total proteinuria or albuminuria ($P < 0.001$). This finding concurred with the previous observation that several peptide fragment biomarkers of the UPSr have a high misfolding potential (*10*).

Urine congophilia associates with immunoreactivity for oligomeric epitopes of prototype misfolded proteins

We used three quaternary structure antibodies previously validated to identify mutually exclusive epitopes of known amyloidogenic proteins (*14*). The A11 polyclonal antibody detects generic, sequence-independent conformational epitopes on cytotoxic PFOs that appear to be antiparallel β sheet structures, including β barrels and β cylindrins (*23*–*26*). The αAPF polyclonal antibody recognizes generic, sequence-independent epitopes on APF conformations that appear to be β barrels and are more mature and thus less cytotoxic than generic PFOs (*13*). The OC antibody detects parallel, in-register fibril conformations of mature fibrils and soluble fibrillar oligomers (*15*). We performed protein-normalized dot blots on a subset of 234 consecutive urine specimens from P-CRL ($n = 57$), crHTN ($n = 16$), mPE ($n = 33$), and sPE ($n = 128$) women. We found higher A11 immunoreactivity in sPE compared to P-CRLs and crHTN women ($P < 0.001$, Fig. 4A). Compared to P-CRL and crHTN, both sPE and mPE women had significantly elevated urine immunoreactivity for αAPF at enrollment (sPE: $P < 0.001$ and $P = 0.021$, respectively; mPE: $P = 0.004$ and $P = 0.035$, respectively; Fig. 4B). As shown in Fig. 4C, we noted heterogeneity in A11 and αAPF immunoreactivity, with some specimens (S3 and S4) reacting equally to both antibodies, and others (S2) predominantly to one. These results can be explained by recent findings suggesting a role for PFOs as precursors for APF formation (*14*). The OC antibody had no detectable reactivity. Collectively, these results indicated the presence of both PFOs and APFs, but not fibrillar oligomers or mature fibrils in the urine of women with PE. However, not all sPE women with urine congophilia displayed detectable APF or PFO immunoreactivity. Figure 4D displays a 3D plot of the A11 and αAPF immunoreactivity along with congophilia measurement for each urine specimen included in our analysis. Whereas most non-MIDPE samples ($n = 73$, green circles) clustered together close to the graph's origin, the MIDPE specimens ($n = 161$, red squares) scattered substantially along the three axes, illustrating the large heterogeneity among urine PFO, APF, and congophilia. Within the MIDPE group, CRR correlated significantly with PFO ($r = 0.268$, $P < 0.001$) but not APF immunoreactivity ($r = 0.128$, $P = 0.106$). The selective

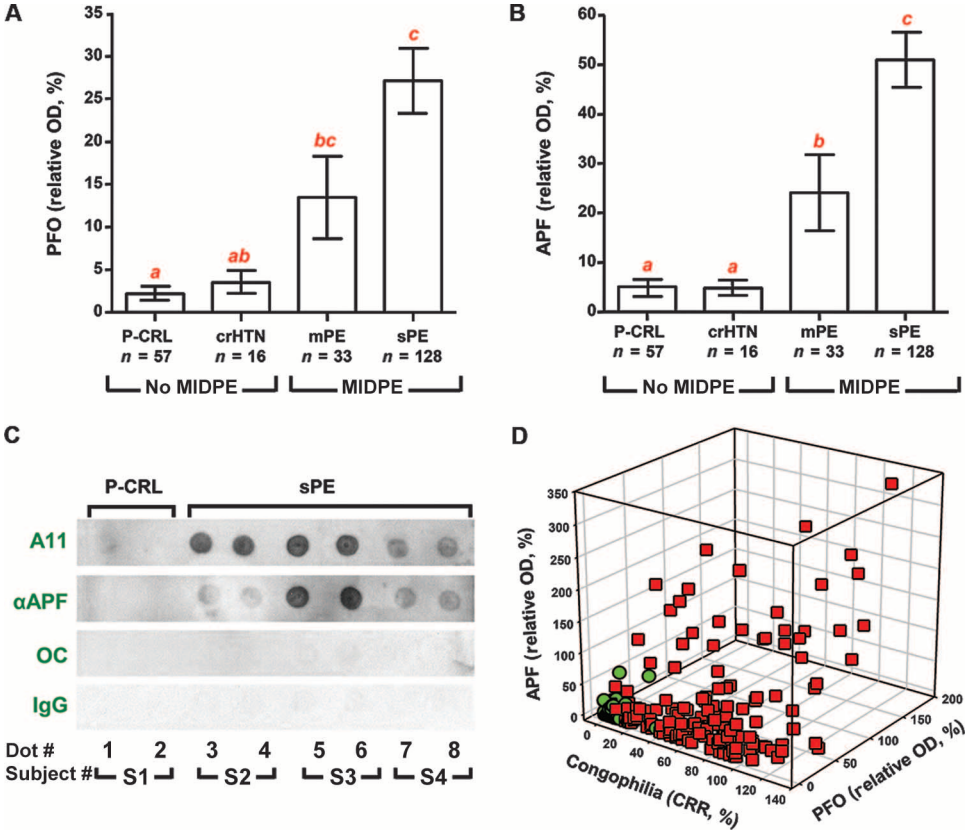

Fig. 4. Urine oligomeric immunoreactivity and relationship with PE severity. (**A** to **C**) Urine samples of P-CRL subjects (n = 57) and of women with crHTN (n = 16), mPE (n = 33), or sPE (n = 128) were tested by immuno-dot blots for the presence and amounts of PFOs (detected by A11 antibody: A and C), APFs (detected by αAPF antibody: B and C), and mature fibrils (detected by the OC antibody: C). Cases were selected consecutively from the feasibility and cross-sectional validation phases on the basis of both enrollment and outcome criteria: no MIDPE for P-CRL and crHTN groups and MIDPE for mPE and sPE. (C) Immuno-dot blots from representative P-CRL (S1: dots 1 and 2) and sPE subjects (S2: dots 3 and 4, S3: dots 5 and 6, S4: dots 7 and 8) showing the presence of PFOs (reactivity for A11 antibody: S2 ≥ S1 > S3) and APFs (reactivity for αAPF antibody: S2 > S3 > S1) in sPE urine. The OC antibody did not detect fibril immunoreactivity above the nonspecific level of rabbit immunoglobulin G (IgG). (**D**) Three-dimensional (3D) plot of urine congophilia (x axis), PFO (y axis), and APF immunoreactivities (z axis). MIDPE cases: red squares (n = 161); non-MIDPE cases: green circles (n = 73). (A and B) Groups sharing at least one common red letter are not statistically different at $P > 0.05$ (data presented as means and SEM, one-way ANOVA). Exact P values are provided in table S6. OD, optical density.

correlation of CRR with PFO remained significant (P = 0.002) after adjustment for GA and total proteinuria (urine P/C ratio) in multiple regression. Compared to women with absent urine PFO immunoreactivity, patients who tested positive had significantly higher systolic (P = 0.002) and diastolic (P = 0.020) blood pressures, and more severe clinical manifestations of the hypertensive syndrome ($P < 0.001$). These analyses remained significant after correction for GA and proteinuria (systolic blood pressure, P = 0.001; diastolic blood pressure, P = 0.027; clinical manifestations, P = 0.003).

Congophilic material isolated from PE urine contains fibrillar nanoscale structures with amyloid-like microscopic features

We developed a protocol for CR-assisted precipitation of urine samples to further characterize the congophilia of PE. When the sPE precipitate was visualized by polarized microscopy (Fig. 5A), green birefringent particles (see inset) were observed. At transmission electron microscopy (TEM; Fig. 5, B and C), the particles appeared as fibrillar arborescent conformations tangled together in larger electrodense structures. These structures were absent in P-CRL specimens processed and imaged in parallel (Fig. 5D). Negative stain TEM (Fig. 5, E and F) showed the monofibrils as elongated filaments of ~50- to 60-nm diameter with smooth, rounded ends (asterisks). Except for the thicker diameter, this overall microscopic appearance of the congophilic precipitate from sPE urine closely resembled that of fibrils extracted from amyloid-laden tissues stained with CR (*27*, *28*).

Immunologic and proteomic analysis of congophilic material in PE urine reveals a heterogeneous protein component

The term "misfoldome" has recently emerged to describe any collection of misfolded proteins (*29*). In our previous proteomics study (*10*), we found that discriminatory biomarkers of the UPSr represented nonrandom cleavage fragments of SERPINA1 and albumin. Because it was specifically SERPINA1's known propensity to aggregate that led us to think about protein misfolding in PE, the next logical step was to search for footprints of SERPINA1 and albumin in urine congophilic material. Figure 5G (left panel) shows a representative SERPINA1 Western blot of two sPE urine samples (lanes U1 and U2) and their corresponding CR precipitate (lanes P1 and P2). As shown, the CR pellet was remarkably enriched in SERPINA1 immunoreactivity, with the ladder pattern indicating the predominance of SERPINA1 fragments compared to the intact precursor (expected mass ~57 kD, blue arrow). A nonspecific Coomassie stain of the same samples (Fig. 5G, right panel) illustrated that the process of CR-assisted precipitation results in a change in banding pattern, implying that only some peptides in sPE urine have CR affinity, and SERPINA1 fragments are part of this family. Figure 5H (left panel) is a representative Western blot for albumin, which illustrates an sPE urine sample before (U1) and after (P1) CR-assisted precipitation. As shown, the intact albumin precursor (expected mass ~67 kD, blue arrow) and higher–molecular weight aggregates appeared predominant relative to albumin fragments. These experiments confirmed that CR precipitates from sPE urine have a protein component, which, although heterogeneous, does not appear random. The protein component was further validated by TEM immunolabeling with anti-SERPINA1 (Fig. 5I) and anti-albumin (Fig. 5J) antibodies. The pattern observed at double immuno-TEM (Fig. 5K) indicated that SERPINA1 coexists

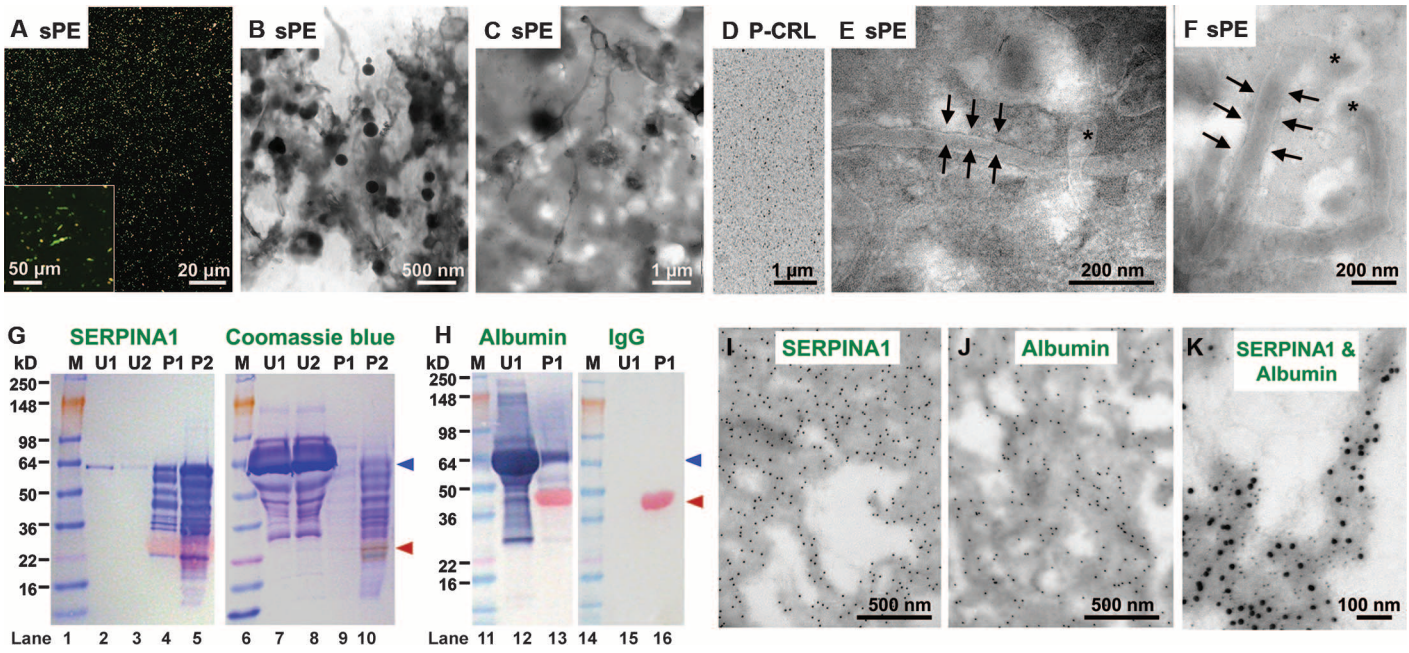

Fig. 5. Microscopic and immunoreactive features of congophilic aggregates isolated from urine of women with sPE. (**A** to **C**) Congophilic precipitate from representative sPE urine specimens imaged in polarized light (A) or by TEM (B and C). (**D**) A urine specimen from a normal pregnant woman (P-CRL) processed identically is shown for comparison. (**E** and **F**) TEM imaging of aggregates after negative staining with uranyl acetate. The edges and dumbbell-shaped tip of a typical fibril are marked by the arrows and asterisks, respectively. SDS–polyacrylamide gel electrophoresis of representative sPE urine specimens (U1 and U2) and their respective CR-assisted precipitates (P1 and P2). (**G** and **H**) Gels were either electroblotted to nitrocellulose membranes (G: lanes 1 to 5 and H: lanes 11 to 16) or stained for total proteins with Coomassie blue (G: lanes 6 to 10). Nitrocellulose membranes were probed with polyclonal antibodies against SERPINA1 (G: lanes 2 to 5) and albumin (H: lanes 12 and 13) or with rabbit IgG (G: lanes 15 and 16). M, molecular weight marker. Blue arrowheads mark the position expected for the nonaggregated intact SERPINA1 (G) and albumin (H), respectively. Antibody-specific bands resolved above the mass marked by the blue arrow represent SDS-resistant aggregates of SERPINA1 (G: lane 5) and albumin (H: lanes 12 and 13). Red arrowheads mark the position of CR dye, which detaches from the protein aggregates in reducing conditions. The blots were detected colorimetrically with 3,3,5,5-tetramethylbenzidine (TMB). (**I** and **J**) TEM imaging of sPE CR aggregates after immunogold labeling of SERPINA1 (I) or albumin (J). (**K**) Double immunogold labeling for albumin (5-nm particles) and SERPINA1 (10-nm particles).

with albumin in the CR precipitates, which supports the idea of heterologous coaggregation.

To determine what other proteins may be represented in CR precipitate, we applied proteomics techniques to select sPE cases (n = 4) from the feasibility cohort. In addition to blood pressure and proteinuria, these cases presented with at least two of the following: eclampsia (n = 2), diaphoresis (n = 1), hemolysis, elevated liver enzymes, and low platelet count syndrome (n = 2) and/or IUGR (n = 2). Aside from SERPINA1 and albumin, which were confirmed by liquid chromatography–tandem mass spectrometry (LC-MS/MS), other represented identities were IgG κ-free light chain (κFLC), ceruloplasmin, and interferon-inducible protein 6-16 (IFI6 also known as G1P3) (table S4). These identities were validated by Western blotting of CR precipitates prepared from women in the validation cohort, selected on the basis of availability of sufficient sample volume (n = 60). Representative confirmatory Western blots for κFLC (expected electrophoretic mass ~25 to 30 kD), ceruloplasmin (~150 kD), G1P3 (~30 kD), SERPINA1 (~57 kD), and albumin (~67 kD) in urine CR precipitates from three women with preterm sPE are shown in fig. S2. Collectively, these results suggest that the congophilic material of sPE women contains proteoforms derived from fragments and/or aggregates of multiple proteins. Moreover, the congophilic aggregates from sPE patients share a nonrandom pattern of immunoreactive proteoforms from at least five different proteins. κFLC, ceruloplasmin, and G1P3 had their most predominant immunoreactive band at the expected molecular size of the intact protein, which supports their intrinsic aggregation propensity even in the nonfragmented state.

Unlike κFLC and ceruloplasmin, which have been previously reported to undergo pathologic aggregation with relevance for several human conformational disorders (*30*–*32*), G1P3 has not been previously investigated for participation in amyloid structures. We performed an in silico analysis of the amyloidogenic potential for the three G1P3 isoforms resulting from alternative splicing (*33*, *34*). Within the G1P3 sequence, we noted an unusually high number of aggregation-prone segments ("hot spots") (*35*). The AGGRESCAN algorithm predicted that G1P3 has an aggregation propensity that exceeds that of $A\beta_{42}$, with the shortest isoform (G1P3a) being the most amyloidogenic (Na4vSS: G1P3a: 13.6 versus $A\beta_{42}$: 6.4; fig. S3 and table S5) (*36*).

PE urine contains aggregated APP proteoforms

It is well known that fibrillar amyloid proteins are resistant to proteolysis by trypsin (*37*). This led us to consider the possibility that our proteomics approach, which relied on fingerprinting of tryptic cleavage peptides, might have missed important proteins, such as APP, in the urine congophilic material.

APP is a ubiquitously expressed protein with three main isoforms (APP770, APP751, and APP695) generated through alternative splicing of the *APP* gene (*38*, *39*). In the normal metabolic pathway, APP is

first cleaved by α-secretase, rather than β-secretases, to release a soluble N-terminal fragment (sAPPα) (*40*). The cleaved sAPPα is nonamyloidogenic and functions as a growth factor promoting cell survival, proliferation, and migration (*41*). However, cleavage of APP by β-secretase and subsequently by λ-secretase (Fig. 6A) releases the short Aβ peptide, which is a major constituent of congophilic senile plaques (*38*, *39*). Because of its high propensity for oligomerization and self-assembly, Aβ has direct pathological roles in inducing oxidative stress and neurodegeneration linked to Alzheimer's disease (*40*, *42*).

On the basis of the above knowledge, we searched for APP fragments in the CR precipitate of urine samples retrieved from women with sPE. We performed Western blotting with the ALZ90 monoclonal antibody, which recognizes residues 511 to 608 in a domain specific to APP (*43*, *44*), to demonstrate the presence of APP fragments (Fig. 6B, lanes P1 to P3) in these samples. The most conspicuous bands migrated between 60 and 90 kD, with a consistent banding pattern among sPE cases. This pattern was either absent or modified in spPE cases (P4 to P7), which supports the pathogenic difference between these two clinically overlapping syndromes associated with pregnancy. Because all samples shown in Fig. 6B had NR-CRR levels, we propose that urine congophilia may constitute a collection of misfolded proteins that includes APP fragments.

We next investigated by Western blot the presence of APP fragments in crude urine specimens of healthy P-CRL (n = 8) and sPE (n = 16) women, with well-characterized monoclonal antibodies raised against an array of epitopes on the APP sequence: ALZ90, DE2B4 (reactive with an epitope within residues 1 to 17 of the Aβ region), 22C11 (reactive with an N-terminal epitope of APP, sAPP, and the structurally related protein APLP-2) (*43*), and MAB5354 (reactive with an epitope in the KPI domain) (*45*). In Fig. 6C, we show that similar to the CR precipitate, crude sPE urine specimens (U3 to U8) exhibited intense ALZ90 immunoreactivity. DE2B4 detected a similar immunoreactivity pattern with ALZ90, albeit of lower intensity. Because the nonspecific cross-reactivity of human albumin with the two anti-APP monoclonal antibodies was ruled out (Fig. 6D, shown for DE2B4), the likeliest explanation for the banding pattern revealed by ALZ90 and DE2B4 in sPE urine was APP fragmentation and/or coaggregation of APP fragments with other proteins. The latter possibility was substantiated by the decrease in intensity of the prominent 64-kD band upon treatment of sPE urine with Cibacron blue, a protein binding dye with high affinity for albumin (fig. S4, A and B). The 22C11 antibody (Fig. 6E) detected immunoreactive urine proteins in both P-CRL (U1 and U2) and sPE (U3 to U8) at the expected molecular weight for mature sAPP (~130 kD, blue arrow). Yet, sPE urine contained an additional band (~110 kD, asterisk), likely representing immature sAPP (*41*). Some sPE women with intense ALZ90 and DE2B4 immunoreactivity (lanes U3, U7, and U8) had less prominent 22C11 sAPP bands. We used an enzyme-linked immunosorbent assay (ELISA) that detects total N-terminal cleaved sAPP to confirm the presence of APP proteoforms in urine and serum of both P-CRL and sPE women. sPE women (n = 66) had higher fractional excretion of sAPP compared to P-CRLs (n = 44)

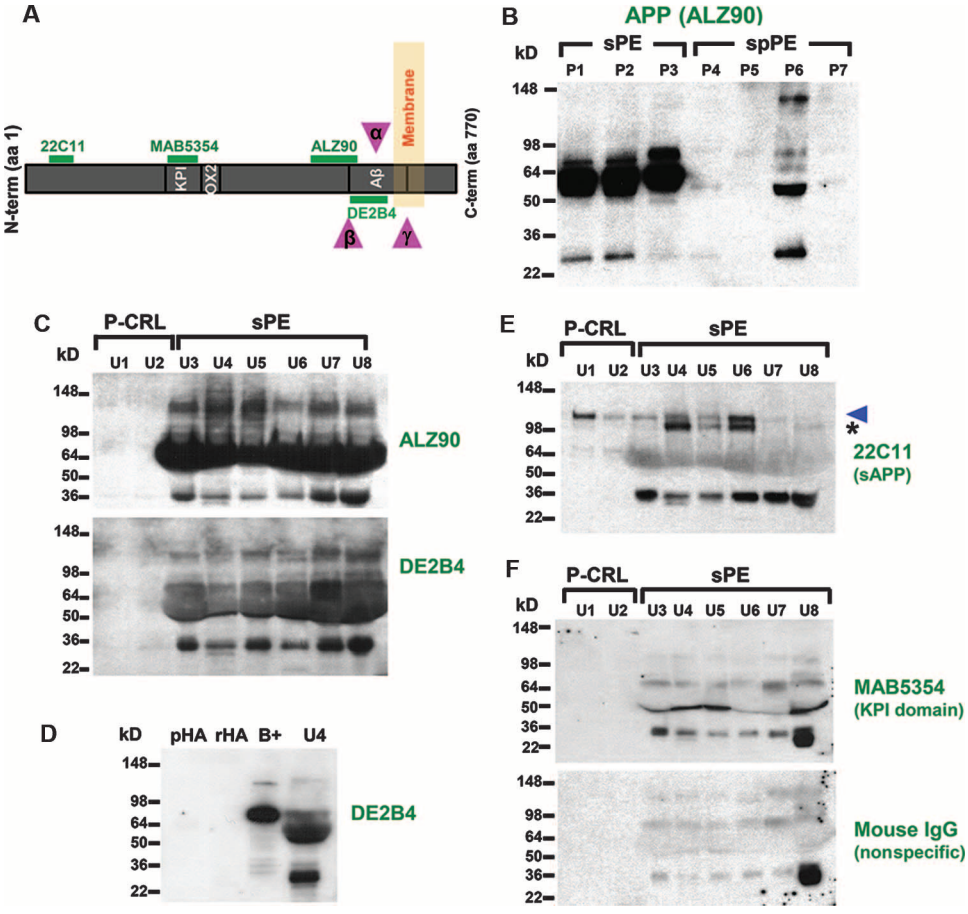

Fig. 6. APP proteoforms in urine of women with sPE. (**A**) Diagram showing the functional domains of APP, major sites of proteolytic cleavage by APP secretases (α, β, and γ), and relative position of the epitopes recognized by the monoclonal antibodies used in this study. The Ox2 and Kunitz protease inhibitor (KPI) domains are present in longer forms of APP. Aβ is a proteolytic fragment of APP released through action of β- and γ-secretases. (**B**) Western blot of congophilic precipitates isolated from urine of women with early-onset sPE (P1 to P3) or with PE (spPE) superimposed on either crHTN (P4 and P5) or chronic nephropathy (P6 and P7). (**C**) Western blots for APP immunoreactivity in crude urine samples of preterm women with uncomplicated pregnancies (P-CRL: U1 and U2) and women with early-onset sPE (U3 to U8). Identical membranes were probed with two antibodies binding to the Aβ sequence: ALZ90 and DE2B4. (**D**) Albumin cross-reactivity was ruled out by the negative reaction with human albumin [purified (pHA) and recombinant albumin (rHA)]. Positive reactivity was seen with Alzheimer's brain homogenate (B+) and sPE urine (sample U4 shown). (**E** and **F**) Western blots for APP proteoforms demonstrated with C terminus and KPI domain anti-APP antibodies. The blue arrowhead marks the expected position of sAPP (~120 kD). Immature sAPP forms are expected to have faster mobility (asterisk). An identical blot was probed with isotype mouse IgG.

(fig. S5A, $P = 0.032$), associated with lower serum sAPP concentration (fig. S5B, $P = 0.009$).

sAPP isoforms containing the KPI domain (APP770 and APP751) function as anti-proteases and are generically referred to as protease nexin-II (APP-KPI/PN2) (*46*). Similar to SERPINA1, APP-KPI/PN2 potently inhibits serine proteases, including trypsin and coagulation factors acting as suicide substrates (*46*). Fragments of APP-KPI/PN2 that include the KPI domain are highly amyloidogenic (*47*, *48*). Figure 6F demonstrates that urine specimens of sPE women contain an APP fragment (~47 kD) specifically detected by the MAB5354 (KPI domain) antibody. However, compared to DE2B4, MAB5354 immunoreactivity and hence the contribution of APP751 isoform appeared to be small (fig. S6, A and B). In summary, mature sAPP proteoforms are normal urine constituents in healthy pregnancies. The relatively low serum sAPP, higher fractional excretion, and high amount of fragmented APP proteoforms in sPE urine point to a possible derangement in the APP proteolytic processing pathway in sPE.

Human placenta expresses mRNA for APP and for prototype α-, β-, and γ-secretases

Placenta is central to the pathophysiology of PE. Because cellular processing of APP is a well-characterized sequence of enzymatic cleavages, we investigated the placental mRNA expression of total APP and of prototype APP-processing enzymes: α-secretases (ADAM10 and ADAM17), β-secretases (BACE1 and BACE2), and γ-secretases (PSEN1 and PSEN2). By quantitative real-time polymerase chain reaction, we determined that the human placenta expresses mRNA for APP and for α-, β-, and γ-secretases, with higher expression preterm versus term for APP, ADAM10, ADAM17, BACE2, PSEN1, and PSEN2 (Fig. 7, A to D). The relative abundance of the α-secretase ADAM10 was significantly higher than that of ADAM17, both preterm ($P = 0.001$) and term ($P = 0.009$, Fig. 7B). The amplification signal for the β-secretase BACE1 was only weakly detected in both preterm and term placenta. This was in contrast to BACE2, which was expressed at significantly higher levels, especially in preterm placenta ($P < 0.001$ versus term, Fig. 7C). Compared to α- and β-secretases, γ-secretases had overall lower mRNA expression. The mRNA for PSEN1 was significantly higher compared to that of PSEN2 in preterm ($P = 0.007$), but not in term, placentas ($P = 0.209$), where both γ-secretases were expressed at low amounts (Fig. 7D). The villous trophoblast mRNA content of ADAM10 ($P < 0.001$) and BACE2 ($P < 0.001$) was significantly higher in sPE compared to GA-matched placental tissues of women with idiopathic preterm birth (iPTB) (Fig. 7E). A comparison among the same groups showed decreased BACE1 mRNA levels in sPE ($P = 0.021$, Fig. 7E). No significant changes in the mRNA expression were noted for ADAM17, PSEN1, PSEN2, or APP ($P > 0.05$ for all) (Fig. 7F).

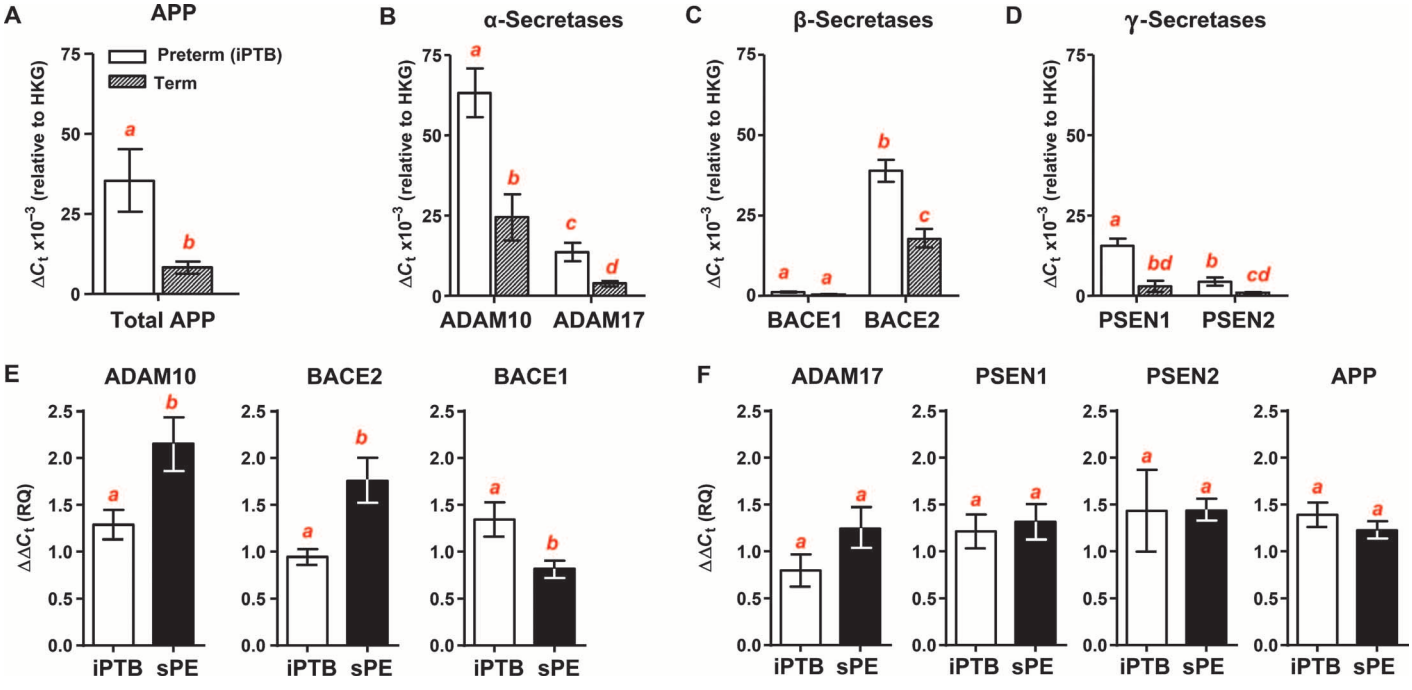

Fig. 7. mRNA expression of APP and prototype APP-processing enzymes in human placenta. (**A**) mRNA expression of APP in placental villous tissue of non-preeclamptic preterm (iPTB, $n = 8$) and term (elective C-section, $n = 5$) pregnancies. The primer and probe pair did not discriminate among APP transcript variants. (**B** to **D**) Relative mRNA amounts of prototype enzymes involved in APP metabolism: (B) α-secretases (ADAM10 and ADAM17), (C) β-secretases (BACE1 and BACE2), and (D) γ-secretases [presenilin-1 (PSEN1) and presenilin-2 (PSEN2)]. ΔC_t values were reported relative to expression of the housekeeping genes (HKG) β-2 microglobulin and ribosomal protein L30 (A to D). (**E**) Relative quantitation (RQ) of transcripts found differentially expressed between placental villous tissues of pregnancies complicated by iPTB ($n = 8$) or early-onset sPE ($n = 8$). (**F**) Relative quantitation of transcripts found statistically unchanged. $\Delta\Delta C_t$ values were reported relative to a reference placental RNA pool (E and F). Statistical comparisons were performed among groups on each graph. Groups sharing at least one common red letter are not statistically different at $P > 0.05$. Data are presented as means and SEM (A, E, and F: *t* tests; B to D: two-way ANOVA followed by Holm-Sidak tests to adjust for multiple comparisons). Exact *P* values are provided in table S6.

sPE associates with placental deposition of amyloid-like ALZ90-positive aggregates

We identified intense 22C11 (N terminus) APP immunoreactivity in the basal plate and chorionic villi of iPTB placentas (Fig. 8A). Decidual cells stained more intensely than extravillous trophoblasts, whereas in the placental villi, endothelial cells (Fig. 8A, inset, open head arrows) and cytotrophoblasts (closed head arrows) stained more conspicuously than the surrounding stroma. There were notable differences in 22C11 staining patterns between sPE and iPTB placentas. In sPE, decidual cells stained positive at almost the same intensity compared to iPTB, but the distribution of the 22C11 decidual cells was more scattered and had a distorted morphology (Fig. 8B). Intense staining of acellular filamentous aggregates was observed in the maternal intervillous spaces on sPE sections (Fig. 8B, inset, arrowhead).

The pattern of ALZ90 antibody staining (specific for Aβ amyloid plaques) (*43*, *44*) was different from that observed with 22C11. ALZ90-positive areas were scarce in preterm iPTB tissues, and when present, they localized more often to the decidua (Fig. 8C) rather than to placental villi, where histological immunoreactivity was virtually absent (Fig. 8C, inset). Conversely, in sPE placentas, ALZ90 staining was more prominent in both the basal plate (Fig. 8D) and villous areas (Fig. 8E), giving an overall piecemeal appearance of the placenta. ALZ90 positivity localized to punctate (Fig. 8E, inset) or flaky acellular material aggregated into plaques (Fig. 8F). ALZ90-positive plaques were more frequently observed in areas affected by fibrinoid-like degeneration. Still, not all fibrinoid-like material was ALZ90-positive. At H&E staining, the ALZ90-positive material had a characteristic purple proteinaceous appearance different from the surrounding eosinophilic fibrinoid (Fig. 8G). Incubation with mouse IgG confirmed staining specificity (Fig. 8H). The ALZ90-positive endovascular material was immunoreactive for G1P3 and frequently noted in areas traditionally described morphologically as placental calcifications, which we confirmed by alizarin S staining (fig. S7).

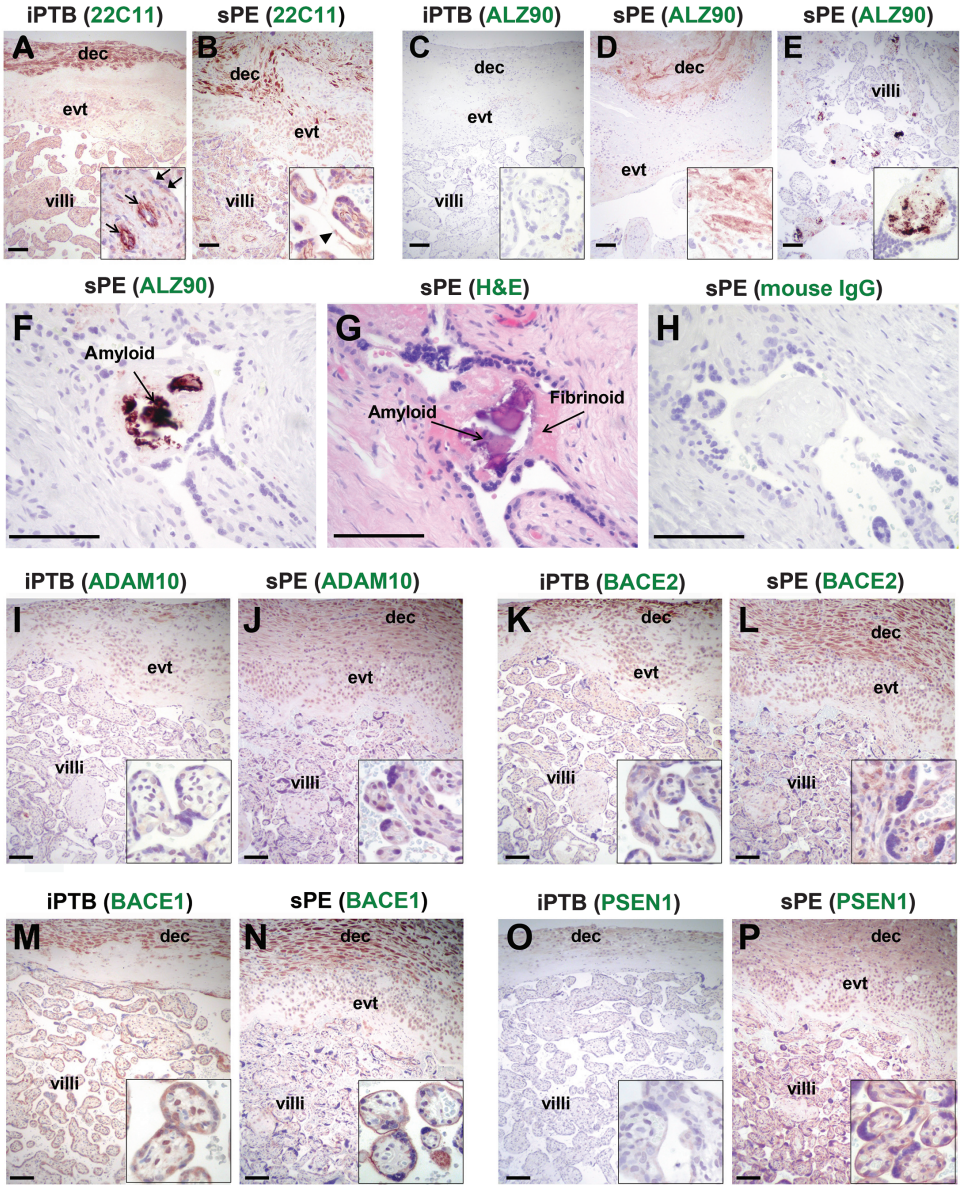

Fig. 8. Immunolocalization of APP and prototype APP-processing enzymes in human placenta. (**A** to **E**) Representative photomicrographs of APP immunostaining using either the 22C11 (N terminus of APP) antibody or ALZ90 (epitope spans into the Aβ domain) in placental villous tissue from pregnancies complicated by either iPTB (A and C) or medically indicated PTB for sPE (B, D, and E). Note the differences in staining pattern with the two antibodies within the decidua (dec), extravillous trophoblasts (evt), and villous portion of the placenta (villi). Scale bars, 200 μm (large panels) or 50 μm (insets). (**F** to **H**) Serial sections from a representative case of sPE with intrauterine growth restriction (IUGR) illustrating proteinaceous aggregates resembling amyloid plaques. APP immunostaining with ALZ90 antibody (F), hematoxylin and eosin (H&E) (G), and isotype mouse IgG as negative control (H). Scale bars, 100 μm. (**I** to **L**) Photomicrographs representative of immunostaining for secretases found up-regulated at the mRNA level in sPE compared to iPTB placentas (ADAM10: I and J; BACE2: K and L). (**M** to **P**) Photomicrographs representative of immunostaining for secretases involved in Aβ generation (BACE1: M and N; PSEN1: O and P) in iPTB (M and O) and sPE (N and P) placentas. Scale bars, 200 μm (large panels) or 50 μm (insets). Note the difference in villous immunostaining for BACE1 and overall staining intensity for PSEN1.

Human placenta expresses immunoreactivity for prototype α-, β-, and γ-secretases

Compared to iPTB placentas, sPE placentas expressed more ADAM10 ($P = 0.017$; Fig. 8, I and J) and BACE2 ($P = 0.007$; Fig. 8, K and L). In sPE, villous ADAM10 immunoreactivity localized predominantly to cytotrophoblasts (Fig. 8J, inset), whereas the β-secretase BACE2 was more ubiquitously expressed among the placental cell populations,

including villous cytotrophoblasts, syncytiotrophoblast, and villous stromal cells (Fig. 8L, inset). Human placenta was found to display positive immunostaining for BACE1. In iPTB placentas, decidual cells and cytotrophoblasts showed most of the positive BACE1 staining (Fig. 8M). A change in BACE1 expression pattern was observed in sPE villi, with prominent BACE1 presence in the syncytiotrophoblast layer that appeared to surround the edge of the villi (Fig. 8N, inset). sPE placentas showed regional differences in BACE1 staining intensity (fig. S8). Areas in proximity of placental infarcts were observed to have the most marked syncytiotrophoblast staining. With respect to the γ-secretase PSEN1, iPTB placenta had virtually absent staining in villous cytotrophoblasts or syncytiotrophoblast (Fig. 8O, inset). Conversely, the sPE syncytiotrophoblast showed notable staining for PSEN1 ($P = 0.038$; Fig. 8P, inset), which together with BACE1 represent two key enzymes involved in APP processing via the amyloidogenic pathway.

DISCUSSION

On the basis of its low prevalence in the general population and limited knowledge on etiology, PE is categorized as a rare "orphan disease" (*49*). Yet, PE is a feared complication of pregnancy. Key challenges for identification of effective therapies for PE are discovery of the factors responsible for hypertension, proteinuria, and late lifetime cardiovascular complications (*50*). An important factor hindering research progress in PE is that the pathophysiologic process leading to hypertension and proteinuria is believed to begin long before clinical manifestations of the disease. In the absence of a gold standard diagnostic test that identifies the pathophysiologic process in its incipient phase, it is difficult to know with certainty which patient harbors latent PE. Moreover, because clinical signs and symptoms of PE are nonspecific, it is likely that PE is a reflection of a larger spectrum of hypertensive and/or proteinuric disorders empirically placed under the same syndromic umbrella (*3*, *51*). Last, although placenta is known to play a central pathophysiologic role in PE, a clear correlation between placental lesions and disease severity cannot be established (*52*). Thus, one can never be certain whether the disease has or has not commenced.

We previously reported that PE women excrete nonrandom fragments of SERPINA1 and albumin (*10*). The presence of aggregated SERPINA1 proteoforms was also identified in the placenta of sPE women (*10*). Consistent with the observation that urine SERPINA1 fragments have the propensity to misfold and aggregate supramolecularly (*11*), we extended our studies to explore the hypothesis that PE reflects a sum of pathological effects associated with the above two processes. In the present investigation, our first step was to investigate whether PE women exhibit urine congophilia. This feature is a well-recognized marker of protein instability and misfolding (*20*) and has been widely used as a postmortem histologic indicator of Aβ deposits in Alzheimer's brain (*53*). Although the mechanism of CR binding to the amyloid fibril surface is not fully understood, it is known that this phenomenon is reliant on the β sheet conformation of the amyloid structure (*20*, *54*). This structural arrangement allows the perfectly planar CR molecule to intercalate between the grooves of β sheets, where electrostatic or hydrophobic interactions irreversibly stabilize it (*54*). As shown, retention of CR by urine proteins and the increased fluorescence and spectral shift of the urine aggregates strengthens the argument that in PE, urine CR dye binds to proteins that are unfolded, are misfolded, and/or have amyloid-like characteristics. We also used conformational state–dependent antibodies to show that most urine specimens from sPE cases contain more PFOs and APFs, as determined by A11 and αAPF immunoreactivities, as compared to fibrils detected by the OC antibody. Soluble, immature amyloid oligomers from different amyloid-forming sequences are increasingly recognized as the primary toxic species responsible for disease pathogenesis (*13*). The PE phenotype could be therefore the result of the presence of soluble and highly cytotoxic oligomeric assemblies to which, at least in part, the clinical heterogeneity of PE may be linked.

The translational relevance of our research is that urine congophilia could serve as a rapid diagnostic and prognostic marker for PE. Our analysis demonstrated that assessment of urine congophilia with the CRD test performs better at predicting MIDPE than the current clinical protocols for rapid assessment of proteinuria (dipstick). These observations have immediate clinical applicability, because rapidly assessing proteinuria may avoid a missed opportunity to prevent PE-related maternal mortality in low-resource settings, which is where most PE-related deaths occur (*55*). Urine dipsticks are not readily available in many developing countries and are associated with false-positive and false-negative results (*56*). Our data provide additional explanation for the poor performance of dipsticks and 24-hour urine proteinuria alone in estimating maternal complications in women with PE (*57*). The dipstick's colorimetric reagent (tetrabromophenol blue) detects only a fraction of the proteins excreted in PE urine. Two components identified in the congophilic precipitate extracted from PE urine (κFLC and fragmented albumin) are notorious in their zero dipstick reaction (*58*). κFLCs are also known to aggregate in a nonlinear fashion subsequent to chemical denaturation (*58*), which is frequently the process used for clinical assessment of proteinuria in 24-hour urine collections by turbidimetry (including in our clinical setting). Therefore, both the dipstick and turbidimetric methods may underestimate the extent of proteinuria and render a false-negative diagnosis for PE. We do not suggest that CRD test should replace the 24-hour urine protein collection as the gold standard for assessment of proteinuria when such test is available or able to be completed. However, both currently used laboratory methods for estimation of proteinuria are unable to provide important qualitative information on misfolded proteins, which, on the basis of our findings, may be a process more closely related to the pathophysiology of PE compared to total proteinuria. All the above may explain why the CRD test was superior to the dipstick at predicting MIDPE and why some women with 24-hour proteinuria below the PE cutoff displayed NR-CRR tests.

An important consideration is that the predictive values reported for the validation cohort in this study are specific to the population targeted for enrollment (consecutive patients presenting at an academic referral hospital in the United States) and would not necessarily be applicable to different populations of women or to health care settings with different obstetric standards for MIDPE.

It is well recognized that blood pressure and/or proteinuria are not ideal tests to discriminate PE and its phenotypic variants from pregnancy-associated hypertensive conditions with different etiology than PE. The CRD test proved valuable for discriminating spPE from uncontrolled crHTN. In addition, several nonproteinuric atypical PE cases displayed NR-CRR. This suggests that at least some cases deemed atypical share a common pathophysiology with traditional PE. Finally, the CRD test had better predictive value for PE compared to P/C ratio,

urine angiogenic factors sFlt-1 and PlGF, and their ratio. The CRD test performed equally well with the urine proteomics analysis, likely because the process of protein fragmentation and misfolding in PE are mechanistically related.

In our longitudinal cohort, most women who eventually developed PE displayed NR-CRR values weeks before clinically overt PE. Some patients had urine congophilia at a GA <20 weeks, which by definition is the earliest gestational point when PE manifests clinically. Collectively, these observations imply that the underlying mechanism leading to urine congophilia in PE likely occurs early in the asymptomatic phase and worsens progressively.

The urinary congophilic material of sPE women had footprints of multiple proteins such as albumin, SERPINA1, κFLC, ceruloplasmin, G1P3 (IFI6), and APP. Whether these proteoforms coaggregate in the maternal circulation or in kidney remains unknown. SERPINA1, κFLC, and APP have been detected in amyloids of various conformational diseases with different pathogenic mechanisms. The pathogenic link among the composing proteoforms, 3D conformations, and clinical manifestations of the PE syndrome requires further investigation. Because PE is a human-specific disorder and for some of the identified proteins (G1P3) no murine homolog exists, the task will be challenging (*59*).

Before this study, the expression of APP or APP-processing enzymes has not been investigated in either placenta or fetal membranes. Therefore, we felt compelled to determine whether the presence of aggregated Aβ is accompanied by dysregulation in APP-processing pathways in PE. We first identified that APP mRNA was abundantly expressed in both placenta and decidua. The elevated fractional excretion of sAPP, up-regulation of major APP-processing enzymes, and increased deposition of aggregated Aβ in the villous trophoblast point to an excessively active APP-processing pathway in PE placentas. It further suggests an insufficient or defective placental or systemic clearance of misfolded proteins. Clearance mechanisms of misfolded proteins are not aggregate-specific (*60*) and have a finite ability to eliminate damaged proteins. Alteration of the clearance mechanisms may explain the frequent association of the PE syndrome with preexisting conditions characterized by increased load of misfolded proteins (diabetes, chronic autoimmune, cardiovascular or renal diseases, and advanced age) (*61*, *62*). This indicates that such women may start pregnancy with an inadequate protein misfolding clearing reserve.

Our data showed that among the enzymes of the secretory pathway, ADAM10 and BACE2 were transcriptionally up-regulated in sPE placentas. Although BACE1 and PSEN1 have been implicated in Aβ generation, our study found lower placental mRNA expression for these two enzymes. Yet, immunohistochemistry demonstrated an up-regulation in their protein expression in PE trophoblasts. This discrepancy is not surprising, because BACE1 expression is driven by complex transcriptional and nontranscriptional mechanisms, including alternative splicing, posttranslational modifications, cellular trafficking, and degradation (*63*). Hence, the role of an increased histological staining of BACE1 in PE placentas warrants further investigation.

Pregnancy encompasses a short time period compared to the human life span. Within this window, the maternal organism is required to adapt to an incredible molecular crowding created by the growing fetus and placenta. If one considers that pregnancy-induced physiologic proteinuria (*64*) represents an adaptive mechanism to prevent protein crowding and aggregation, the pathologic proteinuria of PE could be viewed not only as a loss of integrity to the glomerular filtration barrier but also as an additional way to eliminate larger aggregates. Studying how different mammalian species resolve the process of pregnancy-related protein crowding may open inroads for further understanding conformational disorders. On the basis of our findings, targeted therapy for attenuation of protein fragmentation and aggregation in women at risk for PE may arrest or prevent development of the syndrome if administered at an early stage.

MATERIALS AND METHODS

Included in Supplementary Materials.

SUPPLEMENTARY MATERIALS

www.sciencetranslationalmedicine.org/cgi/content/full/6/245/245ra92/DC1
Materials and Methods
Fig. S1. Quantitative relationship of urine congophilia with 24-hour proteinuria.
Fig. S2. Western blot validation of protein identities associated with the PE misfoldome.
Fig. S3. Comparative aggregation prediction of interferon-inducible protein 6-16 (G1P3) isoforms.
Fig. S4. Effect of albumin depletion on ALZ90 immunoreactivity in preeclamptic urine.
Fig. S5. Fractional excretion and serum concentration of sAPP measured by ELISA.
Fig. S6. Patterns of APP immunoreactivity in preeclamptic urine.
Fig. S7. Immunolocalization of ALZ90 and G1P3 epitopes in calcified Alzheimer's disease–like plaques in preeclamptic placenta.
Fig. S8. Patterns of immunoreactivity for β-secretases BACE1 and BACE2 in preeclamptic placenta.
Table S1. Demographic, clinical, and outcome characteristics of women whose urine samples were used in the feasibility phase (n = 80).
Table S2. Demographic, clinical, and outcome characteristics of pregnant women whose urine samples were used in the cross-sectional validation phase (n = 516).
Table S3. Comparative prognostic accuracy for prediction of MIDPE among subjects in the validation phase with known pregnancy outcomes (n = 563).
Table S4. Summary of LC-MS/MS protein identification results.
Table S5. Aggregation parameters of interferon-inducible protein 6-16 (IFI6 or G1P3).
Table S6. Exact P values (provided as an Excel file).
References (*65*–*70*)

REFERENCES AND NOTES

1. K. S. Khan, D. Wojdyla, L. Say, A. M. Gülmezoglu, P. F. Van Look, WHO analysis of causes of maternal death: A systematic review. *Lancet* **367**, 1066–1074 (2006).
2. *ACOG Practice Bulletin 33. Diagnosis and Management of Preeclampsia and Eclampsia* (American College of Obstetricians and Gynecologists, Washington, DC, 2002).
3. B. M. Sibai, C. L. Stella, Diagnosis and management of atypical preeclampsia-eclampsia. *Am. J. Obstet. Gynecol.* **200**, 481.e1–481.e7 (2009).
4. B. Sibai, G. Dekker, M. Kupferminc, Pre-eclampsia. *Lancet* **365**, 785–799 (2005).
5. A. A. Shamshirsaz, M. Paidas, G. Krikun, Preeclampsia, hypoxia, thrombosis, and inflammation. *J. Pregnancy* **2012**, 374047 (2012).
6. B. M. Sibai, Biomarker for hypertension-preeclampsia: Are we close yet? *Am. J. Obstetrics Gynecol.* **197**, 1–2 (2007).
7. W. Ramma, I. A. Buhimschi, G. Zhao, A. T. Dulay, U. A. Nayeri, C. S. Buhimschi, A. Ahmed, The elevation in circulating anti-angiogenic factors is independent of markers of neutrophil activation in preeclampsia. *Angiogenesis* **15**, 333–340 (2012).
8. R. Boij, J. Svensson, K. Nilsson-Ekdahl, K. Sandholm, T. L. Lindahl, E. Palonek, M. Garle, G. Berg, J. Ernerudh, M. Jenmalm, L. Matthiesen, Biomarkers of coagulation, inflammation, and angiogenesis are independently associated with preeclampsia. *Am. J. Reprod. Immunol.* **68**, 258–270 (2012).
9. U. D. Anderson, M. G. Olsson, K. H. Kristensen, B. Åkerström, S. R. Hansson, Review: Biochemical markers to predict preeclampsia. *Placenta* **33** (Suppl.), S42–S47 (2012).
10. I. A. Buhimschi, G. Zhao, E. F. Funai, N. Harris, I. E. Sasson, I. M. Bernstein, G. R. Saade, C. S. Buhimschi, Proteomic profiling of urine identifies specific fragments of SERPINA1 and albumin as biomarkers of preeclampsia. *Am. J. Obstet. Gynecol.* **199**, 551.e1–551.e6 (2008).
11. J. A. Huntington, Serpin structure, function and dysfunction. *J. Thromb. Haemost.* **9** (Suppl. 1), 26–34 (2011).

12. P. Frid, S. V. Anisimov, N. Popovic, Congo red and protein aggregation in neurodegenerative diseases. *Brain Res. Rev.* **53**, 135–160 (2007).
13. R. Kayed, E. Head, J. L. Thompson, T. M. McIntire, S. C. Milton, C. W. Cotman, C. G. Glabe, Common structure of soluble amyloid oligomers implies common mechanism of pathogenesis. *Science* **300**, 486–489 (2003).
14. R. Kayed, A. Pensalfini, L. Margol, Y. Sokolov, F. Sarsoza, E. Head, J. Hall, C. Glabe, Annular protofibrils are a structurally and functionally distinct type of amyloid oligomer. *J. Biol. Chem.* **284**, 4230–4237 (2009).
15. R. Kayed, E. Head, F. Sarsoza, T. Saing, C. W. Cotman, M. Necula, L. Margol, J. Wu, L. Breydo, J. L. Thompson, S. Rasool, T. Gurlo, P. Butler, C. G. Glabe, Fibril specific, conformation dependent antibodies recognize a generic epitope common to amyloid fibrils and fibrillar oligomers that is absent in prefibrillar oligomers. *Mol. Neurodegener.* **2**, 18 (2007).
16. M. A. Smith, P. L. Richey, R. N. Kalaria, G. Perry, Elastase is associated with the neurofibrillary pathology of Alzheimer disease: A putative link between proteolytic imbalance and oxidative stress. *Restor. Neurol. Neurosci.* **9**, 213–217 (1996).
17. M. A. Salameh, J. L. Robinson, D. Navaneetham, D. Sinha, B. J. Madden, P. N. Walsh, E. S. Radisky, The amyloid precursor protein/protease nexin 2 Kunitz inhibitor domain is a highly specific substrate of mesotrypsin. *J. Biol. Chem.* **285**, 1939–1949 (2010).
18. M. Halimi, Y. Dayan-Amouyal, Z. Kariv-Inbal, Y. Friedman-Levi, T. Mayer-Sonnenfeld, R. Gabizon, Prion urine comprises a glycosaminoglycan-light chain IgG complex that can be stained by Congo red. *J. Virol. Methods* **133**, 205–210 (2006).
19. R. P. Linke, Highly sensitive diagnosis of amyloid and various amyloid syndromes using Congo red fluorescence. *Virchows Arch.* **436**, 439–448 (2000).
20. W. E. Klunk, R. F. Jacob, R. P. Mason, Quantifying amyloid β-peptide (Aβ) aggregation using the Congo red-Aβ (CR–Aβ) spectrophotometric assay. *Analyt. Biochem.* **266**, 66–76 (1999).
21. R. Guidotti, D. Jobson, *Detecting Preeclampsia: A Practical Guide* (World Health Organization, Geneva, 2005).
22. C. S. Buhimschi, E. R. Norwitz, E. Funai, S. Richman, S. Guller, C. J. Lockwood, I. A. Buhimschi, Urinary angiogenic factors cluster hypertensive disorders and identify women with severe preeclampsia. *Am. J. Obstet. Gynecol.* **192**, 734–741 (2005).
23. Y. Yoshiike, R. Kayed, S. C. Milton, A. Takashima, C. G. Glabe, Pore-forming proteins share structural and functional homology with amyloid oligomers. *Neuromol. Med.* **9**, 270–275 (2007).
24. Y. Yoshiike, R. Minai, Y. Matsuo, Y. R. Chen, T. Kimura, A. Takashima, Amyloid oligomer conformation in a group of natively folded proteins. *PLOS One* **3**, e3235 (2008).
25. E. Cerf, R. Sarroukh, S. Tamamizu-Kato, L. Breydo, S. Derclaye, Y. F. Dufrêne, V. Narayanaswami, E. Goormaghtigh, J. M. Ruysschaert, V. Raussens, Antiparallel β-sheet: A signature structure of the oligomeric amyloid β-peptide. *Biochem. J.* **421**, 415–423 (2009).
26. A. Laganowsky, C. Liu, M. R. Sawaya, J. P. Whitelegge, J. Park, M. Zhao, A. Pensalfini, A. B. Soriaga, M. Landau, P. K. Teng, D. Cascio, C. Glabe, D. Eisenberg, Atomic view of a toxic amyloid small oligomer. *Science* **335**, 1228–1231 (2012).
27. T. Shirahama, A. S. Cohen, High-resolution electron microscopic analysis of the amyloid fibril. *J. Cell Biol.* **33**, 679–708 (1967).
28. J. D. Sipe, A. S. Cohen, Review: History of the amyloid fibril. *J. Struct. Biol.* **130**, 88–98 (2000).
29. H. Z. Malina, System in biology leading to cell pathology: Stable protein-protein interactions after covalent modifications by small molecules or in transgenic cells. *J. Biomed. Sci.* **18**, 7 (2011).
30. N. E. Hellman, S. Kono, H. Miyajima, J. D. Gitlin, Biochemical analysis of a missense mutation in aceruloplasminemia. *J. Biol. Chem.* **277**, 1375–1380 (2002).
31. P. G. Winyard, R. C. Hider, S. Brailsford, A. F. Drake, J. Lunec, D. R. Blake, Effects of oxidative stress on some physiochemical properties of caeruloplasmin. *Biochem. J.* **258**, 435–445 (1989).
32. S. Kumar, A. Dispenzieri, J. A. Katzmann, D. R. Larson, C. L. Colby, M. Q. Lacy, S. R. Hayman, F. K. Buadi, N. Leung, S. R. Zeldenrust, M. Ramirez-Alvarado, R. J. Clark, R. A. Kyle, S. V. Rajkumar, M. A. Gertz, Serum immunoglobulin free light-chain measurement in primary amyloidosis: Prognostic value and correlations with clinical features. *Blood* **116**, 5126–5129 (2010).
33. J. M. Kelly, A. C. Porter, Y. Chernajovsky, C. S. Gilbert, G. R. Stark, I. M. Kerr, Characterization of a human gene inducible by α- and β-interferons and its expression in mouse cells. *EMBO J.* **5**, 1601–1606 (1986).
34. M. G. Turri, K. A. Cuin, A. C. Porter, Characterisation of a novel minisatellite that provides multiple splice donor sites in an interferon-induced transcript. *Nucleic Acids Res.* **23**, 1854–1861 (1995).
35. F. Chiti, C. M. Dobson, Protein misfolding, functional amyloid, and human disease. *Annu. Rev. Biochem.* **75**, 333–366 (2006).
36. O. Conchillo-Solé, N. S. de Groot, F. X. Avilés, J. Vendrell, X. Daura, S. Ventura, AGGRESCAN: A server for the prediction and evaluation of "hot spots" of aggregation in polypeptides. *BMC Bioinformatics* **8**, 65 (2007).
37. M. F. Knauer, B. Soreghan, D. Burdick, J. Kosmoski, C. G. Glabe, Intracellular accumulation and resistance to degradation of the Alzheimer amyloid A4/β protein. *Proc. Natl. Acad. Sci. U.S.A.* **89**, 7437–7441 (1992).
38. D. Goldgaber, M. I. Lerman, O. W. McBride, U. Saffiotti, D. C. Gajdusek, Characterization and chromosomal localization of a cDNA encoding brain amyloid of Alzheimer's disease. *Science* **235**, 877–880 (1987).
39. J. Kang, B. Müller-Hill, Differential splicing of Alzheimer's disease amyloid A4 precursor RNA in rat tissues: $PreA4_{695}$ mRNA is predominantly produced in rat and human brain. *Biochem. Biophys. Res. Commun.* **166**, 1192–1200 (1990).
40. B. De Strooper, R. Vassar, T. Golde, The secretases: Enzymes with therapeutic potential in Alzheimer disease. *Nat. Rev. Neurol.* **6**, 99–107 (2010).
41. A. Schmitz, R. Tikkanen, G. Kirfel, V. Herzog, The biological role of the Alzheimer amyloid precursor protein in epithelial cells. *Histochem. Cell Biol.* **117**, 171–180 (2002).
42. C. Haass, D. J. Selkoe, Cellular processing of β-amyloid precursor protein and the genesis of amyloid β-peptide. *Cell* **75**, 1039–1042 (1993).
43. H. J. Clarris, B. Key, K. Beyreuther, C. L. Masters, D. H. Small, Expression of the amyloid protein precursor of Alzheimer's disease in the developing rat olfactory system. *Brain Res. Dev. Brain Res.* **88**, 87–95 (1995).
44. V. Muresan, N. H. Varvel, B. T. Lamb, Z. Muresan, The cleavage products of amyloid-β precursor protein are sorted to distinct carrier vesicles that are independently transported within neurites. *J. Neurosci.* **29**, 3565–3578 (2009).
45. K. Bordji, J. Becerril-Ortega, O. Nicole, A. Buisson, Activation of extrasynaptic, but not synaptic, NMDA receptors modifies amyloid precursor protein expression pattern and increases amyloid-β production. *J. Neurosci.* **30**, 15927–15942 (2010).
46. T. Oltersdorf, L. C. Fritz, D. B. Schenk, I. Lieberburg, K. L. Johnson-Wood, E. C. Beattie, P. J. Ward, R. W. Blacher, H. F. Dovey, S. Sinha, The secreted form of the Alzheimer's amyloid precursor protein with the Kunitz domain is protease nexin-II. *Nature* **341**, 144–147 (1989).
47. L. Ho, K. Fukuchi, S. G. Younkin, The alternatively spliced Kunitz protease inhibitor domain alters amyloid β protein precursor processing and amyloid β protein production in cultured cells. *J. Biol. Chem.* **271**, 30929–30934 (1996).
48. M. Barrachina, E. Dalfó, B. Puig, N. Vidal, M. Freixes, E. Castaño, I. Ferrer, Amyloid-β deposition in the cerebral cortex in dementia with Lewy bodies is accompanied by a relative increase in AβPP mRNA isoforms containing the Kunitz protease inhibitor. *Neurochem. Int.* **46**, 253–260 (2005).
49. Rare Disease Act of 2002; http://www.gpo.gov/fdsys/pkg/PLAW-107publ280/html/PLAW-107publ280.htm [accesed 10 January 2013].
50. E. F. Funai, Y. Friedlander, O. Paltiel, E. Tiram, X. Xue, L. Deutsch, S. Harlap, Long-term mortality after preeclampsia. *Epidemiology* **16**, 206–215 (2005).
51. F. H. Harlow, M. A. Brown, The diversity of diagnoses of preeclampsia. *Hyperten. Preg.* **20**, 57–67 (2001).
52. P. Zhang, M. Schmidt, L. Cook, Maternal vasculopathy and histologic diagnosis of preeclampsia: Poor correlation of histologic changes and clinical manifestation. *Am. J. Obstet. Gynecol.* **194**, 1050–1056 (2006).
53. A. J. Howie, D. B. Brewer, Optical properties of amyloid stained by Congo red: History and mechanisms. *Micron* **40**, 285–301 (2009).
54. C. Wu, Z. Wang, H. Lei, W. Zhang, Y. Duan, Dual binding modes of Congo red to amyloid protofibril surface observed in molecular dynamics simulations. *J. Am. Chem. Soc.* **129**, 1225–1232 (2007).
55. UNICEF-WHO, *Antenatal Care in Developing Countries: Promises, Achievements and Missed Opportunities* (World Health Organization, Geneva, 2003).
56. N. Murray, C. S. Homer, G. K. Davis, J. Curtis, G. Mangos, M. A. Brown, The clinical utility of routine urinalysis in pregnancy: A prospective study. *Med. J. Austr.* **177**, 477–480 (2002).
57. S. Thangaratinam, A. Coomarasamy, F. O'Mahony, S. Sharp, J. Zamora, K. S. Khan, K. M. Ismail, Estimation of proteinuria as a predictor of complications of pre-eclampsia: A systematic review. *BMC Med.* **7**, 10 (2009).
58. V. Maisnar, M. Tichy, J. Stulik, J. Vavrova, B. Friedecky, V. Palicka, J. Spirkova, L. Zaloudkova, L. Hernychova, J. Spacilova, T. Buchler, R. Hajek, The problems of proteinuria measurement in urine with presence of Bence Jones protein. *Clin. Biochem.* **44**, 403–405 (2011).
59. N. Parker, A. C. Porter, Identification of a novel gene family that includes the interferon-inducible human genes *6–16* and *ISG12*. *BMC Genomics* **5**, 8 (2004).
60. R. E. Tanzi, R. D. Moir, S. L. Wagner, Clearance of Alzheimer's Aβ peptide: The many roads to perdition. *Neuron* **43**, 605–608 (2004).
61. R. W. Carrell, D. A. Lomas, Conformational disease. *Lancet* **350**, 134–138 (1997).
62. M. R. Hayden, S. C. Tyagi, M. M. Kerklo, M. R. Nicolls, Type 2 diabetes mellitus as a conformational disease. *JOP* **6**, 287–302 (2005).
63. S. L. Cole, R. Vassar, The Alzheimer's disease β-secretase enzyme, BACE1. *Mol. Neurodegen.* **2**, 22 (2007).
64. T. Cornelis, A. Odutayo, J. Keunen, M. Hladunewich, The kidney in normal pregnancy and preeclampsia. *Sem. Nephrol.* **31**, 4–14 (2011).
65. B. M. Sibai, Imitators of severe pre-eclampsia. *Sem. Perinatol.* **33**, 196–205 (2009).
66. R. C. Pattinson, M. Hall, Near misses: A useful adjunct to maternal death enquiries. *Br. Med. Bull.* **67**, 231–243 (2003).

67. Publications Committee, Society for Maternal-Fetal Medicine, B. M. Sibai, Evaluation and management of severe preeclampsia before 34 weeks' gestation. *Am. J. Obstet. Gynecol.* **205**, 191–198 (2011).
68. M. D. Griffin, L. M. Wilson, Y. F. Mok, A. S. Januszewski, A. M. Wilson, C. S. Karschimkus, E. Romas, A. B. Lee, T. Godfrey, M. Wong, L. Clemens, A. J. Jenkins, G. J. Howlett, Thioflavin T fluorescence in human serum: Correlations with vascular health and cardiovascular risk factors. *Clin. Biochem.* **43**, 278–286 (2010).
69. M. Sakono, T. Zako, Amyloid oligomers: Formation and toxicity of Aβ oligomers. *FEBS J.* **277**, 1348–1358 (2010).
70. J. Rybarska, B. Piekarska, B. Stopa, G. Zemanek, L. Konieczny, M. Nowak, M. Król, I. Roterman, A. Szymczakiewicz-Multanowska, Evidence that supramolecular Congo red is the sole ligation form of this dye for L chain lambda derived amyloid proteins. *Folia Histochem. Cytobiol.* **39**, 307–314 (2001).

Acknowledgments: We thank C. Rahner and M. Graham from the Yale Center for Cellular and Molecular Imaging Core Facility for the invaluable assistance with electron microscopy imaging. We also acknowledge the contributions of K. Trotta and G. Cozzini in assisting with the sAPP ELISA and part of the immunohistochemistry experiments. **Funding:** Supported by funds from a Round 5 Grand Challenges Explorations Phase I award entitled "Reducing preeclampsia morbidity through Congo red dot (CRD) test" (principal investigator: I. A. Buhimschi, 2010 to 2012) and funds from the Albert McKern Scholar Award for Perinatal Research, Yale University School of Medicine, entitled "An investigational study of preeclampsia as a protein misfolding disease" (principal investigator: I. A. Buhimschi, 2009 to 2011). Funds from The Research Institute at Nationwide Children's Hospital were used to cover publication-related charges and to support part of the electron microscopy core facility costs. I.M.B. was also supported by NIH grant R01 HL 071944. **Author contributions:** I.A.B. originated the concept. I.A.B. and C.S.B. carried out the project design. C.G.G. developed the conformational state antibodies and participated in the design and interpretation of the experiments involving these antibodies. C.S.B., U.A.N., and E.F.F. participated in the acquisition of clinical specimens from pregnant subjects. I.M.B. participated with clinical samples from nonpregnant subjects and their clinical data. G.Z., L.L.S., U.A.N., A.P., and I.A.B. performed the experiments. I.A.B., C.S.B., C.G.G., and E.F.F. supervised various aspects of the study and contributed to secure funding. I.A.B. and C.S.B. drafted the manuscript. All authors participated in the critical interpretation of the data, reviewed and revised all drafts of the manuscript, and approved the final version. **Competing interests:** I.A.B., C.S.B., and C.G.G. are listed as inventors or co-inventors on patent applications on the use of protein misfolding features in preeclampsia for diagnostic and treatment purposes, some of which are described in this article. **Data and materials availability:** Peptide sequences were uploaded in the Web-accessible Yale Protein Expression Database at http://medicine.yale.edu/keck/proteomics/yped/index.aspx and can be retrieved with access code Xsqoo4.

Submitted 14 February 2014
Accepted 14 May 2014
Published 16 July 2014
10.1126/scitranslmed.3008808

Citation: I. A. Buhimschi, U. A. Nayeri, G. Zhao, L. L. Shook, A. Pensalfini, E. F. Funai, I. M. Bernstein, C. G. Glabe, C. S. Buhimschi, Protein misfolding, congophilia, oligomerization, and defective amyloid processing in preeclampsia. *Sci. Transl. Med.* **6**, 245ra92 (2014).